Nonlinear ESO-based vibration control for an all-clamped piezoelectric plate with disturbances and time delay: design and hardware implementation

Shengquan Li[1, 3*], Luyao Zhang[1], Chaowei Zhu[1], Jinya Su[2], Juan Li[1]

1, College of Electrical, Energy and Power Engineering, Yangzhou University, Yangzhou 225127, China

2, School of Computer Science and Electronic Engineering, University of Essex, Colchester CO4 3SQ, U.K.

3, State Key Laboratory of Mechanics and Control of Mechanical Structures, Nanjing University of Aeronautics and astronautics, Nanjing 210016, China

Abstract**—**Considering the problems of model uncertainties, higher harmonics, uncertain boundary conditions, external excitations and system time delay in practical vibration control system, a novel active vibration control method is proposed to suppress the vibration of a thin plate structure with acceleration sensor and piezoelectric bimorph actuator in this paper. First, a nonlinear extended state observer (NESO)-based controller is designed to ensure the anti-disturbance performance of the structural vibration control system. Then, an enhanced differentiator-based time delay compensation method is introduced to improve the vibration suppression performance of the NESO-based controller. A real time hardware-in-the-loop benchmark for an all-clamped piezoelectric thin plate is designed to verify and compare the performance of the developed controller against conventional ESO-based methods (linear ESO with/without time delay compensation, NESO without time compensation). The best vibration suppression and disturbance rejection performance of the proposed NESO-based controller with an enhanced time delay compensator is verified in the comparative experimental results. This work is able to provide practitioners with vital guidance in designing active vibration control system in the presence of disturbances and time delay.

Index Terms**—**Nonlinear extended state observer (NESO); active vibration control; all-clamped thin plate structure; piezoelectric actuator; time delay; experimental comparison.

[*] **Corresponding author**: Shengquan Li, College of Electrical, Energy and Power Engineering, Yangzhou University, Yangzhou 225127, China E-mail: sqli@yzu.edu.cn

I. INTRODUCTION

The engineering thin plate structures with excellent characteristics (e.g., light weight, large flexibility, simple mechanism, etc.) have been broadly used in practical fields, such as precision instrument shield, ship deck, aircraft skin structure and automobile axle housing (Gozum et al., 2018; Muc et al., 2019). The structural vibration can be easily excited by multifarious disturbances, such as model uncertainties, higher harmonics, unknown external excitations and conditions, when the plate structures are applied to the actual engineering systems. Therefore, how to develop effective vibration suppression is a pressing issue in many industrial fields. The piezoelectric elements (e.g., patch, bimorph and stack) have gradually become alternative choices for structural vibration suppression, since they can conveniently be used as sensors or actuators by embedding into the body thin plate structure due to their unique features of direct and inverse piezoelectric effect (Zhang et al., 2019).

To attenuate the vibration of the actual piezoelectric thin plate structures, feedback-based vibration control methods are generally regarded as the natural choices. Several linear vibration control methods such as LQR/LQG methods, PID controller, and velocity feedback strategies have been applied to the structural vibration suppression, because these methods have a simple framework and can be realized easily (Guzman et al., 2020; Tomas et al., 2018; Ling et al., 2020; Wang et al., 2018; Anik et al., 2018). However, the performance of these linear vibration control methods highly relies on an accurate system model. However, modeling errors inevitably exist due to the diversity of boundary conditions, higher harmonics and uncertain external excitations in practical engineering thin plate structures. A number of active vibration control methods are also proposed to address the challenges of total disturbances and nonlinearity of the piezoelectric structures in the past decade (Yousefpour et al., 2020; Hu and Li, 2018; Kim et al., 2013; Luo et al., 2018; Pu et al., 2019; Qiu and Han, 2009). Although these methods can improve the suppression performance to some extent, it is difficult to reject the total disturbances directly and effectively without an accurate mathematical model of the disturbances and uncertainties. For instance, sliding model control (SMC)-based active vibration control method has a strong anti-disturbance ability, however, the chattering phenomenon and sensitivity to mismatched disturbances have limited its practical applications in structural vibration systems (Qiu et al., 2021; Rezaee et al., 2019; Zhang and Jing, 2020). Therefore, vibration suppression controller for piezoelectric structure should be designed rationally to possess robustness and anti-disturbance ability simultaneously. To address these problems, the disturbance-estimation-based vibration control methods are also proposed to attenuate the system disturbances in piezoelectric structural systems. To this end, several practical and effective composite vibration control techniques based on disturbance estimation have been developed for specific piezoelectric structures (He et al., 2019; Kant and Parameswaran, 2018; Li et al., 2012; Oveisi et al., 2018; Sun et al., 2018; Xu and Li, 2012; Zhang et al., 2019).

In particular, nonlinear-extended-state-observer-based (NESO-based) control method, originally presented by Han, is based on the idea of disturbance estimation and compensation (Han, 2009). In this approach, system disturbances and uncertainties are defined as an extended state variable by introducing the concept of total disturbances, which may include model uncertainties, higher harmonics, uncertain boundary conditions and external excitation. As a special case, linear ESO (LESO) based control method is usually preferred to solve the practical engineering problems, since it has a simple structure and also fewer tuning parameters. In addition, LESO-based control method is increasingly implemented for the vibration suppression of piezoelectric structures due to its high robustness, strong anti-disturbance ability and less requirement on system model knowledge in past decade (Language et al., 2020; Li et al., 2014a, 2014b; Liu et al., 2020; Zhang et al., 2014; Zheng et al., 2014). Although some practical applications in different fields show that nearly the same performance can be achieved by using NESO-based and LESO-based control methods, some theoretical results prove that the control performance of peaking values and noise tolerance of NESO is better than LESO under similar bandwidth tuning parameters (Wu et al., 2020; Zhao and Guo, 2017, 2018). Although LESO and NESO based control methods have been developed for some special engineering problems, their detailed comparison via real-life experiments are still to be performed so that vital guidance can be provided to practitioners in the fields.

Meanwhile, system time delay arising from computational delay and the sampling time of acquisition card is also a serious challenge in structural vibration system. The actual collocated placement of accelerometers and piezoelectric actuators is hard to be realized in practical vibration engineering, which is also an important factor for system time delay. A LESO-based vibration control method is proposed to compensate the time delay caused by the non-collocated placement of the sensor/actuator pair in ref. (Li et al., 2014b), where the vibration suppression experimental results of a piezoelectric stiffness plate show that the predictor-based LESO method can effectively suppress the structural vibration within a certain frequency range. Unfortunately, the control performance of the LESO-based controller with smith predictor may degrade significantly because of the high frequency noise amplification effect of the traditional differentiator. Time delay is also a significant issue in ESO-based control system, and therefore several theoretical and engineering achievements have been introduced to improve the conventional ESO-based control structures for tackling the total disturbances and time delay (Castaneda et al., 2018; Chen et al., 2018, 2019). The polynomial predictor for time delay is introduced to provide the prediction of system input or output, however, the polynomial approximation value should be obtained with a high computation load (Chen et al., 2018). Although the predictor observer (PO) based ESO method is introduced to handle the total disturbances and system delay, the capability of the PO based ESO is only obtained through a qualitative analysis (Ran et al., 2020). Additionally, time delay part is synchronously added at the input channel of ESO to increase the observer bandwidth and enhance the anti-disturbance ability (Geng et al., 2019). The reduced order ESO, whose stability is rigorously analyzed for the linear time invariant case, is proposed to compensate the matched time delay (Pawar et al., 2017). Smith predictor based ESO, utilizing the output predictive value, is another effective time delay compensation control method (Li et al., 2014b, 2021; Liu et al., 2019; Zhang et al., 2020; Zheng and Gao, 2014). It is noted that although many enhanced ESO-based control methods have been proposed for controlling dynamical systems with total disturbances and time delay, synchronously, their performance analysis have not been fully studied and compared. Thus, the advantages and practicability of ESO-based control methods have not been fully demonstrated, and as a result, the practitioners still face difficulties in choosing the appropriate controller for their specific systems.

To this end, this paper aims to deal with the critical issues in structural vibration control system including total disturbances and time delay. Several ESO-based vibration controllers are adopted to suppress the vibration of a thin plate structure with piezoelectric actuator and accelerometer. Additionally, an enhanced time delay compensator is introduced to attenuate the adverse effect of system time delay without amplifying the high frequency harmonic signals. Via profoundly analyzing the performance of different ESO-based controllers, this paper is able to provide vital guidance for practitioners in choosing suitable controller for their vibration engineering fields. The remainder of this paper is organized as follows. The mathematical model of an all-clamped piezoelectric thin plate is described in **Section II**. A NESO-based controller for structural vibration suppression is designed by introducing a time delay compensator to enhance the efficiency of NESO in **Section III**, meanwhile, the stability of the controller-designed is discussed in frequency domain. In **Section IV**, the proposed enhanced time delay compensator for NESO-based (entitled enhanced TDCNESO- based) controller is validated over some existing controllers via a real-time hardware-in-the- loop system of a piezoelectric plate with NI-PCIe6343 acquisition card. Finally, conclusions are drawn in **Section V** with future research discussion.

II. Mathematical Model of an All-clamped Piezoelectric Plate with SID Method

A. *Subspace identification (SID) method for piezoelectric structural vibration*

In Fig. 1, an all-clamped thin plate with piezoelectric patch can be described as a second order mass-damper-stiffness system, when the plate structure is excited by a certain modal frequency input signal. The variables of F_a, V and y_a represent the sum of uncertain forces applied to the plate structure, driven voltage of piezoelectric patch and output of accelerometer, respectively. The whole dynamic equation of the plate can be expressed as the following equation.

$$m\ddot{d} + c\dot{d} + kd = F_a + F_P \tag{1}$$

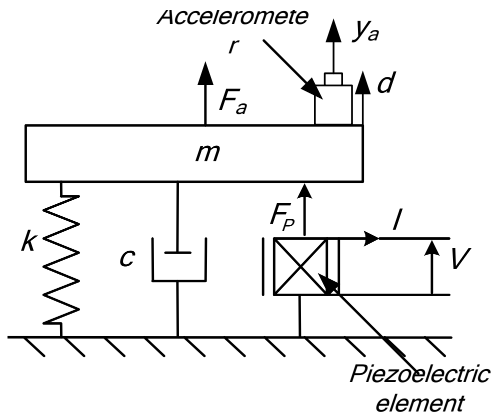

Fig. 1 Diagram of a plate with a piezoelectric actuator

where the parameters m, c, k, d are system mass, system damping, system stiffness and displacement, respectively. The output force value of piezoelectric element can be expressed as $F_P = \eta V$, where the system parameter η relating to the efficiency of converting voltage into force is defined as force factor of piezoelectric actuator. The test value of the modal parameters for the piezoelectric plate structure are related to the short/open circuit frequency of the piezoelectric patches, since these frequencies are easily affected by the temperature of the epoxy resin layer for pasting (Li et al., 2014a, 2014b).

As mentioned above, the piezoelectric plate structure is a typical second order electromechanical system, so its state space model can be achieved by the subspace identification (SID) method. Considering the characteristics of the piezoelectric plate, a SID method is employed to identify the systems parameters in following Eq. (2). This identification method derives the system mathematical model by applying well-conditioned operations like orthogonal projections on Hankel matrices stacked by the input and output data (Overschee and Moor, 1996). A time-invariant linear state-space model identified by SID is formulated as follows.

$$\begin{aligned} \mathbf{x}_{t+1} &= \mathbf{A}\mathbf{x}_t + \mathbf{B}V_t + \mathbf{e}_t \\ d_t &= \mathbf{C}\mathbf{x}_t + \mathbf{D}\mathbf{u}_t + f_t \end{aligned} \tag{2}$$

where $\mathbf{x}_t$ and d_t are the state variable vector and system output at step *t*, respectively. The vectors $\mathbf{e}_t$ and f_t represent the disturbances. The model order is represented by n. $\mathbf{A} \in \Re^{n\times n}$, $\mathbf{B} \in \Re^{n\times 1}$, $\mathbf{C} \in \Re^{1\times n}$ and $\mathbf{D}^{1\times 1}$ are the system matrices. The Block Hankel matrices stacked by input and output data are defined as follows.

$$\mathbf{V}=\begin{bmatrix} V_1 & V_2 & \cdots & V_J \\ V_2 & V_3 & \cdots & V_{J+1} \\ \vdots & \vdots & \vdots & \vdots \\ V_I & V_{I+1} & \cdots & V_{I+J-1} \\ \hline V_{I+1} & V_{I+2} & \cdots & V_{I+J} \\ V_{I+2} & V_{I+3} & \cdots & V_{I+J+1} \\ \vdots & \vdots & \vdots & \vdots \\ V_{2I} & V_{2I+1} & \cdots & V_{2I+J-1} \end{bmatrix}=\begin{bmatrix} \mathbf{V}_p \\ \hline \mathbf{V}_f \end{bmatrix} \tag{3}$$

where the number of block rows I in $\mathbf{V}_p$ and $\mathbf{V}_f$ is given in advance, and $I \geq n$. $J = N - 2I + 1$, where N is the number of available data samples. The subscript symbols *p* and *f* stand for the past and future data, respectively. The output block Hankel matrices $\mathbf{D}$, $\mathbf{D}_p$, $\mathbf{D}_f$ are defined in the same way as Eq. (3). In addition, the matrix $\begin{bmatrix}\mathbf{V}_f^T & \mathbf{V}_p^T & \mathbf{D}_p^T & \mathbf{D}_f^T\end{bmatrix}^T$ can be decomposed as the product of a low triangular matrix **L**, and an orthogonal matrix **Q**.

$$\begin{bmatrix} \mathbf{U}_f \\ \mathbf{U}_p \\ \mathbf{Y}_p \\ \mathbf{Y}_f \end{bmatrix} = \begin{bmatrix} \mathbf{L}_{11} & & & \\ \mathbf{L}_{21} & \mathbf{L}_{22} & & \\ \mathbf{L}_{31} & \mathbf{L}_{32} & \mathbf{L}_{33} & \\ \mathbf{L}_{41} & \mathbf{L}_{42} & \mathbf{L}_{43} & \mathbf{L}_{44} \end{bmatrix} \begin{bmatrix} \mathbf{Q}_1^T \\ \mathbf{Q}_2^T \\ \mathbf{Q}_3^T \\ \mathbf{Q}_4^T \end{bmatrix} \tag{4}$$

Since $\lim_{N\to\infty} \frac{1}{N} span_{col}\left\{\begin{bmatrix}\mathbf{L}_{42} & \mathbf{L}_{43}\end{bmatrix}\right\} = span_{col}\left\{\mathbf{\Gamma}_I\right\}$, the observability matrix $\mathbf{\Gamma}_I$ can be obtained by performing singular value decomposition (SVD) on $\begin{bmatrix}\mathbf{L}_{42} & \mathbf{L}_{43}\end{bmatrix}$.

$$\mathbf{\Gamma}_I = \mathbf{U}_1 \mathbf{S}_1^{1/2}$$

$$\begin{bmatrix}\mathbf{L}_{42} & \mathbf{L}_{43}\end{bmatrix} = \begin{bmatrix}\mathbf{U}_1 & \mathbf{U}_2\end{bmatrix} \begin{bmatrix}\mathbf{S}_1 & \\ & \mathbf{S}_2\end{bmatrix} \begin{bmatrix}\mathbf{V}_1 & \mathbf{V}_2\end{bmatrix}^T \tag{5}$$

where $\mathbf{U}_1 \in \mathbb{R}^{I\times n}$, $\mathbf{S}_1 \in \mathbb{R}^{n\times n}$, $\mathbf{V}_1 \in \mathbb{R}^{J\times n}$ and $\mathbf{\Gamma}_I = \mathbf{U}_1 \mathbf{S}_1^{1/2}$. The model order is determined by the dimension of $\mathbf{S}_1$. For a state space model of a finite dimension, the main diagonal elements of the diagonal matrix $\mathbf{S}_2$ are close to zero. Thus, the system matrices $\mathbf{A}$ and $\mathbf{C}$ can be further estimated as follows.

$$\begin{aligned}\mathbf{A} &= \underline{\mathbf{\Gamma}}_N \overline{\mathbf{\Gamma}}_N \\ \mathbf{C} &= \mathbf{\Gamma}_N(1:K,:)\end{aligned} \tag{6}$$

where $\overline{\mathbf{\Gamma}}_I$ and $\underline{\mathbf{\Gamma}}_I$ can be obtained by removing the first rows and last rows of $\mathbf{\Gamma}_I$, respectively. The matrix $\mathbf{U}_f^{\dagger}$ is the pseudo inverse of matrix $\mathbf{U}_f$, so matrix $\mathbf{M} = \left(\mathbf{\Gamma}_I^{\perp}\right)^T \mathbf{Y}_f \mathbf{U}_f^{\dagger}$ can be defined in the following form.

$$\begin{aligned}\mathbf{M} &= \begin{bmatrix}\mathbf{M}_1 & \mathbf{M}_2 & \cdots & \mathbf{M}_I\end{bmatrix} \\ &= \begin{bmatrix}\mathbf{L}_1 & \mathbf{L}_2 & \cdots & \mathbf{L}_I\end{bmatrix} \times \begin{bmatrix}\mathbf{D} & & & & \\ \mathbf{CB} & \mathbf{D} & & & \\ \mathbf{CAB} & \mathbf{CB} & \mathbf{D} & & \\ \vdots & \vdots & \vdots & \ddots & \\ \mathbf{CA^{I-2}B} & \mathbf{CA^{I-3}B} & \mathbf{CA^{I-4}B} & \mathbf{L} & \mathbf{D}\end{bmatrix}\end{aligned} \tag{7}$$

An explicit equation can be further obtained as follows by algebraic rearrangement.

$$\begin{bmatrix}\mathbf{M}_1 \\ \mathbf{M}_2 \\ \vdots \\ \mathbf{M}_I\end{bmatrix} = \begin{bmatrix}\mathbf{L}_1 & \mathbf{L}_2 & \mathbf{L}_3 & \cdots & \mathbf{L}_I \\ \mathbf{L}_2 & \mathbf{L}_3 & \cdots & \mathbf{L}_I & \\ \mathbf{L}_3 & \cdots & \iddots & & \\ \vdots & \mathbf{L}_I & & & \\ \mathbf{L}_I & & & & \end{bmatrix} \begin{bmatrix}\mathbf{I}_I & 0 \\ 0 & \underline{\mathbf{\Gamma}}_I\end{bmatrix} \begin{bmatrix}\mathbf{D} \\ \mathbf{B}\end{bmatrix} \tag{8}$$

Then the matrices **D** and **B** can be obtained by solving Eq. (8) via the least square method. In addition, the system matrices of Eq. (2) can be obtained by the following experimental setup.

B. System identification

In order to obtain the actual structural mode vibration of the thin plate structure with piezoelectric actuator and accelerometer, the data used for system model identification are acquired by I/O module of NI-PCIe6343 with a sampling time of 0.1ms in Fig. 2. The values of model parameters are summarized in **Table 1**. A vibrator (HEV-20) is used to excite the all-clamped aluminum alloy pate whose dimension is $50\text{cm} \times 50\text{cm} \times 0.1\text{cm}$. The four sides clamped condition is achieved by putting all side ends of the plate between the bars bonded together tightly with several bolts. The hammering method is employed to obtain the first-order mode frequency at 56.17Hz by a LC-02A type force hammer. In addition, in order to determine the accuracy of the experimental results obtained, the theoretical analysis of the structural modes of the all-clamped plate is carried out. For the all-clamped plate, the following mode functions U_m and V_n are selected:

$$U_m = \cosh(\frac{\lambda_m x}{L_x}) - \cos(\frac{\lambda_m x}{L_x}) - \beta_m[\sinh(\frac{\lambda_m x}{L_x}) - \sin(\frac{\lambda_m x}{L_x})] \quad (9)$$

$$V_n = \cosh(\frac{\lambda_n y}{L_y}) - \cos(\frac{\lambda_n y}{L_y}) - \beta_n[\sinh(\frac{\lambda_n y}{L_y}) - \sin(\frac{\lambda_n y}{L_y})] \quad (10)$$

where the coefficients $\beta_i = \dfrac{\cosh(\lambda_i) - \cos(\lambda_i)}{\sinh(\lambda_i) - \sin(\lambda_i)}$, $i = m, n$. The $\cosh(\cdot)$ and $\sinh(\cdot)$ are the hyperbolic cosine and cosine functions. The coefficients λ_m and λ_n satisfy $\cosh(\lambda_i)\cos(\lambda_i) = 1$, $i = m, n$. The natural frequency of the all-clamped plate can be expressed as (Caruso G, 2001):

$$\omega_{mn} = \sqrt{\frac{D}{\rho h}} \bullet \sqrt{\frac{I_1 I_2 + 2I_3 I_4 + I_5 I_6}{I_2 I_6}} \quad (11)$$

where

$$I_1 = \int_0^{L_x} \frac{\partial^4 U_m(x)}{\partial x^4} U_m(x)dx, \; I_2 = \int_0^{L_y} (V_n(y))^2 dy, \; I_3 = \int_0^{L_x} \frac{\partial^2 U_m(x)}{\partial x^2} U_m(x)dx, \quad (12)$$

$$I_4 = \int_0^{L_y} \frac{\partial^2 V_n(y)}{\partial y^2} V_n(y)dy, \; I_5 = \int_0^{L_y} \frac{\partial^4 V_n(y)}{\partial y^4} V_n(y)dy, \; I_6 = \int_0^{L_x} (U_m(x))^2 dx. \quad (13)$$

Therefore, combining theoretical analysis and modal tests, the first-order natural frequency of the all-clamped plate is 56.17Hz. The piezoelectric bimorph (QDA40-10-0.7) at the middle of the thin plate is employed as an actuator for vibration suppression. The dimension of the piezoelectric actuator is 4cm $\times$ 1cm $\times$ 0.08cm in this paper. The vibration response is measured by arranging an accelerator sensor (IEPE-CA-YD-160) near the piezoelectric bimorph after a constant current source regulator (IEPE-YE3821). The control value is obtained by the real-time module of MATLAB/SIMULINK and transmitted to a power amplifier (HVP-300D) via the output module of NI-PCIe6343. The output voltage from NI-PCIe6343 is used to drive the piezoelectric bimorph actuator for vibration suppression.

Table 1 Values of model parameters

The length of the all-clamped plate L_x	0.5m

The width of the all-clamped plate L_y	0.5m
The thickness of the all-clamped plate L_z	0.001m
First resonance frequency f_1	56.17Hz
Blocked capacitance of piezoelectric C_0	125.6nF
Force factor η	0.00158
Stiffness of equivalent piezoelectric element k	37000N/m
Inherent structure damping coefficient c	0.034N/(m·s)
The equivalent rigid mass m	350g

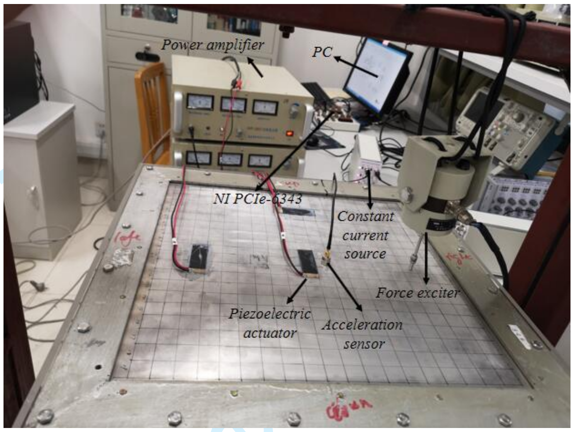

Fig. 2 Experimental set-up of an all-clamped thin plate structure

The inevitable system time delay caused by the mismatched arrangement of sensor/actuator pair and computational delay may decrease the suppression performance or even cause system instability, so the time delay should be considered in deriving the system mathematical model. In this paper, the experimental data of vibrator and accelerometer from acquisition system is used to obtain the time delay coefficient, when the plate structure is excited at 56.17Hz. The Lissajous curves in Fig. 3 can be plotted by using these two acquired input and output signals on X- and Y-coordinates, respectively. It is easy to know that the time delay exists in the vibration control system, because the hysteresis loop resembles an ellipse in Fig. 3. The Lissajous fitting curves for the vibration mode can be smoothed as the following Eq. (14) by trial and error.

$$\begin{aligned} x &= 102\sin(2\pi\omega t) \\ y &= 0.47\sin(2\pi\omega t+\varphi) \end{aligned} \tag{14}$$

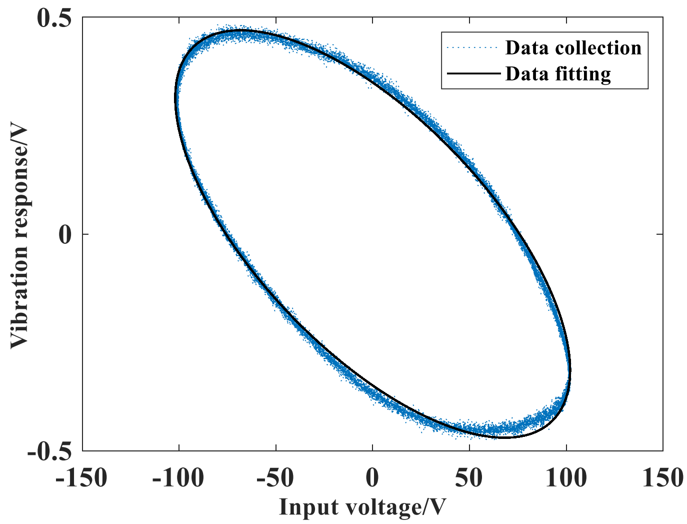

Fig. 3 The Lissajous Curves between the signals measured from power amplifier and accelerometer

where the natural frequency and phase error are $\omega = 56.17$ Hz and $\varphi = 3.98\,rad$, respectively. The Lissajous fitting curves of Eq. (14) can also be obtained in a similar way for experimental data. It is easy to see that the experimental and fitting figures of Lissajous curves for vibration mode are approximately the same in Fig. 3. Additionally, with the above phase lag identification, the time delay τ can be obtained as following Eq. (15).

$$\tau = \frac{1000\varphi}{2\pi\omega} = 11.28ms \tag{15}$$

Therefore, a second order system transfer function with time delay part expressed by Eq. (16) can be deduced from the SID method.

$$Q(s) = \frac{y(s)}{u(s)} = \frac{127.24}{s^2 + 2.957s + 153500} e^{-0.0113s} \tag{16}$$

III. A Novel NESO-based vibration controller design

A. *Design of an enhance delay compensator*

The second-order modal vibration system (16) can be regarded as the product of the delay part and the nominal model part. Although the absolute value of time delay coefficient is small, it can cause control value to lag behind the acceleration signal due to the fast time variation of the whole system. Therefore, the time delay should be considered in the vibration controller design to achieve satisfactory performance. Smith predictive method in Fig. 4 is introduced to convert system (16) into a delay-free system.

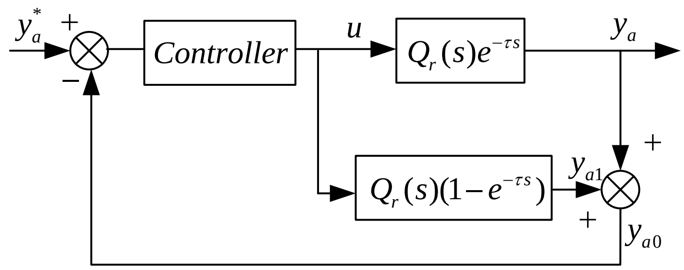

Fig. 4 Smith Predictor for structural vibration system.

Where τ, y_a^*, y_a and u are the time delay coefficient, expected system output, system actual output and input, respectively. The system parameters y_{a0} and y_{a1} are the auxiliary output and the output value of smith predictor, respectively. The proposed Smith prediction method needs to extract the differentiation of the output signal. Considering the noise amplification effect of the traditional differentiator, a new algorithm in the form of Eq. (17) is used to estimate the differential signal.

$$\dot{\hat{y}}_a(t) \approx \frac{y_a(t-\tau_1) - y_a(t-\tau_2)}{\tau_2 - \tau_1}, 0 < \tau_1 < \tau_2 \tag{17}$$

where $\dot{\hat{y}}_a(t)$ is the differentiation estimation, and the τ_1 and τ_2 are time delay coefficients which are approximately equal to τ. More details on the derivation, design and interpretation of the enhance delay compensator can be founded in ref. (Li et al., 2014b, 2021).

B. Enhanced TDCNESO-based controller for an all- clamped piezoelectric plate

The state space equation of the single mode vibration Eq. (16) can be obtained as the following Eq. (18).

$$\begin{cases} \dot{x}_1 = x_2 \\ \dot{x}_2 = -c_2 x_1 - c_1 x_2 + w + c_0 u \\ y = x_1 \end{cases} \tag{18}$$

where w represents the external disturbances. The parameters c_1 and c_2 are the system coefficients. The symbol c_0 is defined as the system control coefficient. The displacement and velocity of the system are defined as state variables by x_1 and x_2, respectively. The total disturbances can be defined as the following Eq. (19).

$$f = -c_2 x_1 - c_1 x_2 - (\hat{c}_0 - c_0)u + w \tag{19}$$

where the polynomial $-c_2x_1 - c_1x_2 - (\hat{c}_0 - c_0)u$ is considered as the internal disturbances, including model errors, system uncertain dynamics and nonlinearity. The symbol $\hat{c}_0$ is the estimation value of the system control gain c_0. A variable $x_3 = f$ is defined as an extended state variable to represent the total disturbances. It is noted that the differential of total disturbances f is global, since f is mainly composed of uncertain dynamics, model errors, external excitations in the piezoelectric plate structure. In addition, the components of total disturbances are the practical physical quantities in the structural vibration system. So system state space model can be rewritten as an extended state equation.

$$\begin{cases} \dot{x}_1 = x_2 \\ \dot{x}_2 = x_3 + \hat{c}_0 u \\ \dot{x}_3 = h \\ y = x_1 \end{cases} \tag{20}$$

Similar to refs. (Han, 2009; Zhao and Guo, 2017, 2018), the NESO corresponding to Eq. (20) can be designed as the following form.

$$\begin{cases} e = z_1 - y_a \\ \dot{z}_1 = z_2 - \beta_{01} e \\ \dot{z}_2 = z_3 - \beta_{02} e + \hat{c}_0 u \\ \dot{z}_3 = -\beta_{03} fal(e, \alpha, \delta) \\ fal(e, \alpha, \delta) = \begin{cases} \dfrac{e}{\delta^{1-\alpha}}, & |e| \le \delta \\ |e|^{\alpha} sign(e), & |e| > \delta \end{cases} \end{cases} \tag{21}$$

where z_1 and z_2 are the estimation values of the system state variables x_1 and x_2, respectively. The estimated error between the actual vibration displacement and its estimation output of NESO is defined as e. The variable z_3 is the estimation of the total unknown disturbances f. The estimation coefficients β_{01}, β_{02} and β_{03}, selected by making a compromise between the vibration control performance and the noise tolerance, are the adjustable gains of the NESO. The parameters α and δ are the filter factor and linear segment interval constant, respectively. So the control input u can be achieved by following Eq. (22) with well-tuned coefficients of NESO by ignoring the estimation error between z_3 and f.

$$u = \frac{u_0 - z_3}{\hat{c}_0} \tag{22}$$

where the traditional PD controller is introduced to suppress the structural vibration in this paper. In addition, the ideal control performance is the structural vibration output in equal to 0, so Eq. (23) is deduced as PD controller with the estimated state variables of NESO (21) for the all-clamped piezoelectric thin plate.

$$u_0 = k_p(0 - z_1) + k_d(0 - z_2) = -k_p z_1 - k_d z_2 \tag{23}$$

where k_p and k_d are the feedback gains of PD controller. The stability of the entire structural vibration system can be guaranteed with the proper PD gains and coefficients of NESO. It is noted that the NESO-based controller (22) cannot directly deal with the time delay, which may be caused by mismatched sensor/actuator pairs, the sampling time of acquisition card, and computational delay in the practical structural vibration control system. Therefore, according to Eqs. (17), (21), (22) and (23), the enhanced time delay compensator for NESO-based (enhanced TDCNESO-based) controller in Eq. (24) is proposed to handle the total disturbances and time delay of the all-clamped piezoelectric thin plate structural vibration system in Fig. 5.

$$\begin{cases} y_{a0} = y_a + \tau \dfrac{s}{\tau_1 \tau_2 s^2 + (\tau_1 + \tau_2)s + 1} y_a \\ e_1 = z_1 - y_{a0} \\ \dot{z}_1 = z_2 - \beta_{01} e_1 \\ \dot{z}_2 = z_3 - \beta_{02} e_1 + \hat{c}_0 u \\ \dot{z}_3 = -\beta_{03} fal(e_1, \alpha, \delta) \\ u = \dfrac{-k_p z_1 - k_d z_2 - z_3}{\hat{c}_0} \end{cases} \tag{24}$$

where y_{a0} is the auxiliary vibration output and e_1 is the estimated error between y_{a0} and the observer output of the NESO. In addition, by using the actual output y_a and its differentiation, the auxiliary variable y_{a0} can be obtained, so the vibration control law (24) does not contain time delay part.

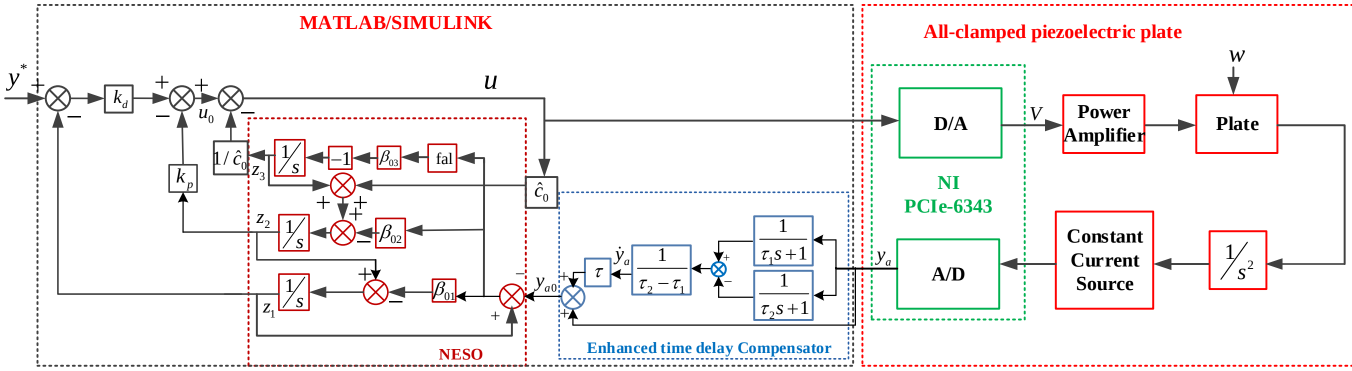

Fig. 5 Schematic structure of vibration suppression system under the enhanced TDCNESO-based controller

C. Stability Analysis

When evaluating the performance of a controller, stability is crucial factor. However, in this paper, both the all-clamped plate-controlled and the NESO-based controller have nonlinear characteristics, which makes it difficult to analyze the stability characteristics of the closed-loop system. Therefore, the system analysis in frequency domain is considered, because compared with the stability criterion in time domain, the Nyquist and Bode diagram in frequency are more vivid and convenient. In order to introduce the system into the frequency, according to the characteristics of time delay, an approximation in frequency domain is used. At the same time, the describing function method is used to solve the nonlinear function “fal”. It is pointed out in ref. (Han, 2009) that when the time constant T of the inertial link is very small, so its transfer function can be approximated to the Laplace transform of the variable delay time T. The mathematical expression is as follows:

$$e^{-Ts} \approx \frac{1}{1+Ts} \tag{25}$$

Therefore, the first equation of Eqs. (24) can be rewritten as follows:

$$\begin{aligned} Y_{a0}(s) &= Y_a(s) + \tau \frac{s}{\tau_1\tau_2 s^2 + (\tau_1+\tau_2)s + 1} Y_a(s) \approx Y_a(s) + \tau s Y_a(s) \\ &= Y_a(s)(1+\tau s) \approx Q(s) e^{\tau s} U(s) \\ &= \frac{127.24}{s^2 + 2.957s + 153500} U(s) \end{aligned} \tag{26}$$

In this way, only ESO with nonlinear function is left in the nonlinear part of the system. Next, the characteristics of the "fal" function will be analyzed, since its describing function will be derived. Firstly, the "fal" function is proposed by Han in ref. (Han, 2009), which is defined as Eq. (21). In this paper, the values of parameters δ and α are 0.01 and 0.5, so a special "fal" function can be considered as follows:

$$fal(e,0.5,0.01)=\begin{cases} e/0.01^{0.5} & |e|\le 0.01 \\ |e|^{0.5}\,\mathrm{sgn}(e) & |e|>0.01 \end{cases} \tag{27}$$

According to reference (Wu and Chen, 2013, 2014), for input whose amplitude is $E(s)$, the description function of "fal" function is denoted as $D(E)$ and its expression is as follows:

$$\begin{aligned} D(E)=&\frac{20}{\pi}\left[\tau-\frac{0.01}{E}\sqrt{1-\left(\frac{0.01}{E}\right)^2}\right]+\frac{2}{\pi E^{0.5}}\left[2\left(\frac{\pi}{2}-\tau\right)\right. \\ &\left.-\frac{1}{2}\left(\frac{\pi}{2}-\tau\right)^3+\frac{1}{16}\left(\frac{\pi}{2}-\tau\right)^5-\frac{19}{6720}\left(\frac{\pi}{2}-\tau\right)^7\right] \end{aligned} \tag{28}$$

where $\tau=\arcsin(0.01/E)$. For $E<0.01$, $D(E)=20$. After derivation, the NLADRC-based control system described by Eqs. (24) can be simplified to the structure shown in Fig. 6 in frequency domain.

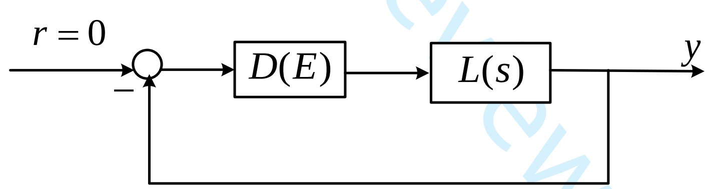

Fig. 6 Simplified structure of vibration suppression system under the TDCNESO-based controller

The expression of $D(E)$ is Eq. (28). The transfer function $L(s)$ is expressed by following Eq. (29):

$$L(s)=\frac{L_{n0}s^2+L_{n1}s+L_{n1}}{L_{d0}s^5+L_{d1}s^4+L_{d2}s^3+L_{d3}s^2+L_{d4}s} \tag{29}$$

The coefficients of $L(s)$ is listed in the Appendix. The characteristic equation of the vibration suppression system under the enhanced TDCNESO-based controller can be obtained as follows:

$$\frac{1}{D(E)}+L(j\omega)=0 \tag{30}$$

Next, the stability of the system is judged by the Nyquist theorem. The parameter values in $L(j\omega)$ are consistent with the actual experiment, as shown in Table 2, and the Nyquist diagram of $L(j\omega)$ is shown in Fig. 7.

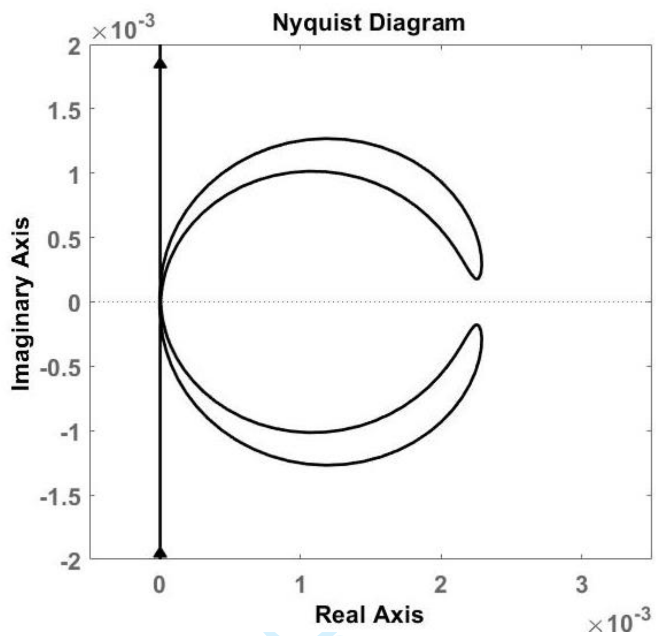

Fig. 7 Nyquist diagram of $L(j\omega)$

It can be found that $D(E)$ is a real function of input amplitude E, So in a real imaginary graph, the trajectory of $D(E)$ will always be on the real axis, and its range is (0,10). Therefore, $-1/D(E)\in(-\infty,-0.1)$. This shows that the curve $L(j\omega)$ does not include the curve $-1/D(E)$. According to Nyquist stability criterion, the closed-loop system is stable.

IV. Experimental Verifications and Analysis

A. *Experimental Set-up*

The thin plate structural vibration is excited by a vibrator, suppressed by a piezoelectric bimorph actuator and measured by an accelerometer. The structure is an all-clamped thin plate (aluminum alloy LY12CZ usually Aircraft-ARJ21). To implement the enhanced time delay compensator for NESO-based vibration controller, an experimental set-up is established in Fig. 2. The sizes of the all-clamped plate and piezoelectric bimorph actuator are consistent with the experimental conditions for system identification. In addition, the types of the accelerometer, acquisition cards, power amplifier, vibrator, constant current source are the same as those in Fig. 2. To implement the proposed enhanced time delay compensator for NESO-based controller, a control structure of the vibration control system based on MATLAB/SIMULINK real-time module is shown in Fig. 5. The vibration signal from the accelerometer is sampled and converted into digital data through the analog-to-digital channel of NI-PCIe6343 board. The output control value of the proposed control method calculated by the MATLAB2017a/ SIMULINK8.9 is amplified to the peak-to-peak voltage of ± 100 v with a power amplifier (HVP-300D) which drives the piezoelectric bimorph to suppress the vibration through a digital-to analog channel in the NI-PCIe6343 board.

B. Experimental Vibration Control

To verify the effectiveness and superiority of the proposed enhanced TDCNESO-based controller, it is compared against the traditional LESO-based, NESO-based, enhanced TDCLESO-based controllers for the all-clamped thin piezoelectric plate. The all-clamped piezoelectric plate is excited by the first modal natural frequency. In order to facilitate the performance comparison of the four ESO-based controllers, the spectrum of the normalized acceleration signal is defined as the following Eq. (31) (Li et al., 2021).

$$\text{The decibel value} = 20\log_{10}(\xi(y_a / y_{a,R})) \tag{31}$$

where the function $\xi(\cdot)$ is defined as the Fourier Transformation. The expected acceleration signal of the whole vibration control system for normalization is expressed by $y_{a,R}$. Considering that the acceleration signal is the measurement in this paper, the value of $y_{a,R}$ is set to 1g as the standard value, i.e., 0dB is equivalent to 1g and -20dB is equivalent to 0.1g.

For a fair comparison, the four ESO-based controllers, i.e., LESO-based, NESO-based, enhanced TDCLESO-based and the proposed enhanced TDCNESO-based controllers, are applied to the same all-clamped piezoelectric plate structure excited by a force vibrator. In addition, the following conditions are chosen for the four ESO-based vibration controllers. (1) The vibrator is excited with the same voltage values at the first natural frequency; (2) the piezoelectric bimorph actuator, accelerometer and force vibrator are always at the same position of the plate surface, respectively; (3) the four kinds of ESO-based controllers are conducted and implemented in MATLAB2017a/ SIMULINK8.9 and NI-PCIe6343 board in Fig. 5. The control parameters of different ESO-based vibration controllers are chosen to achieve a compromise between the vibration suppression performance and noise tolerance, which are summarized in **Table 2**.

Table 2 parameter values of the different ESO-based vibration controllers

Symbols	LESO-based controller	NESO-based controller	Enhanced TDCLESO-based controller	Enhanced TDCNESO-based controller
k_p	20	500	50	1333
k_d	2.5	0.8	2.5	2.7
β_1	36	10	36	10
β_2	432	20	432	20
β_3	1728	35	1728	35
$\hat{c}_0$	0.8	0.3	0.4	0.3
δ		0.01		0.01
α		0.5		0.5

The time and frequency domain responses of the uncontrolled and the four ESO-based vibration controllers for the all-clamped piezoelectric plate structures are shown in Figs. 8 and 9, respectively. It can be seen that the first mode and several high harmonic frequency modes of the all-clamped piezoelectric plate is excited by the first natural frequency signal in Fig. 9. Therefore, the piezoelectric plate structure with the present boundary condition has typical nonlinear vibration characteristics. The driven voltages of the piezoelectric bimorph actuator under the four different ESO-based vibration controllers are shown in Fig.10. The peak-to-peak values of the different ESO-based control input voltages are about 100 V, so the piezoelectric actuator with the voltage can be considered as the second excitation for the effect of the coupling active control signal. In addition, it can be seen from Figs. 8(a)-(b) that the time domain responses of the accelerometer under LESO-based vibration controller is less than one-fifth of the original value without controller. The LESO can effectively estimate and attenuate effects of the total disturbances through feed-forward channel, the LESO-based vibration controller can significantly suppress the structural vibration.

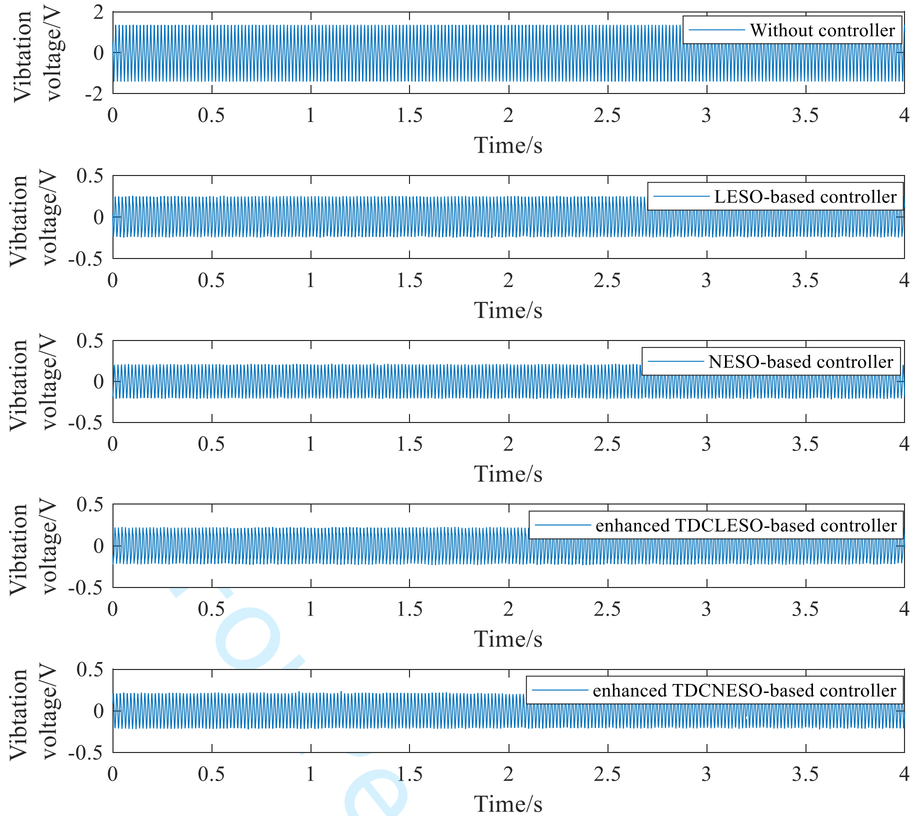

(a) Global response curves

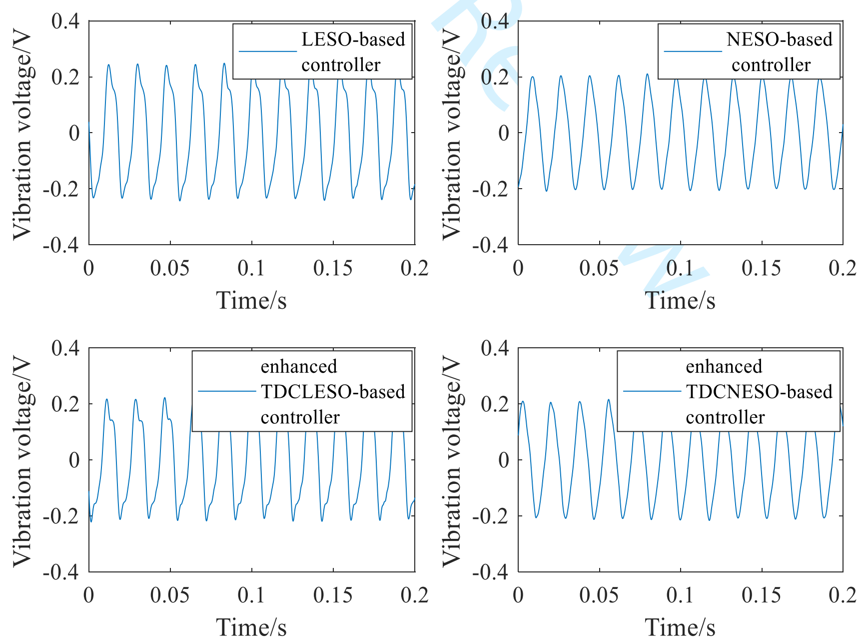

(b) Local response curves

Fig. 8 Vibration suppression performance comparisons in time domain under LESO-based, NESO-based, enhanced TDCLESO-based and the proposed enhanced TDCNESO-based controllers.

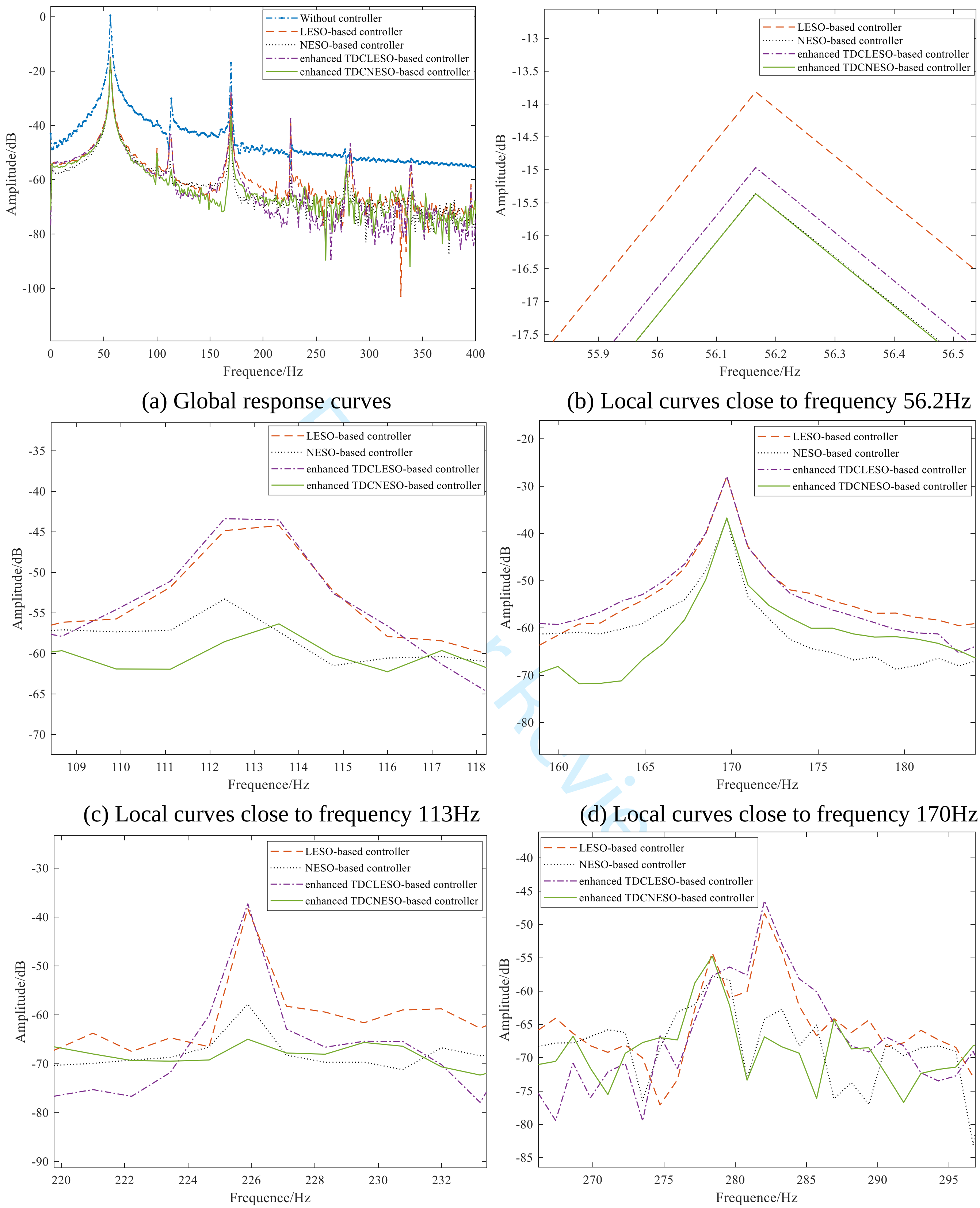

(a) Global response curves

(b) Local curves close to frequency 56.2Hz

(c) Local curves close to frequency 113Hz

(d) Local curves close to frequency 170Hz

(e) Local curves close to frequency 226Hz

(f) Local curves close to frequency 280Hz

Fig. 9 Vibration suppression performance comparisons in frequency domain under LESO-based, NESO-based, enhanced TDCLESO-based and the proposed enhanced TDCNESO-based controllers.

The experimental results in Figs. 8 and 9 (a)-(b) also indicate that the whole vibration suppression performance under the enhanced TDCLESO-based vibration controller is better than that under LESO-based controller, especially at the first natural frequency. Therefore, it can be concluded that the enhanced time delay compensator can effectively eliminate the influence of time delay with lower driven voltages.

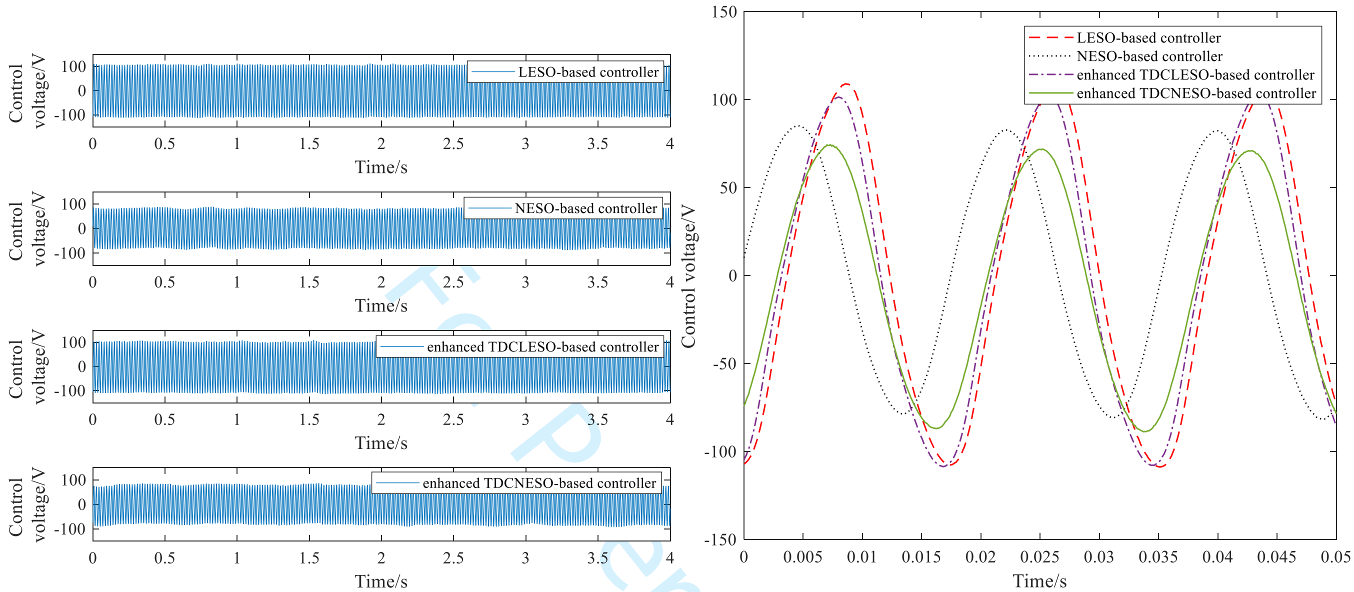

(a) Global curves of the control voltages (b) Local curves of the control voltages

Fig. 10 Piezoelectric bimorph driven voltages under LESO-based, NESO-based, enhanced TDCLESO-based and the proposed enhanced TDCNESO-based controllers

In addition, the vibration amplitude measured by accelerometer is reduced in a wide frequency range in Fig. 9(a). The experimental results in Figs. 8 and 9 show that the performance of the two NESO-based vibration controllers is better than the two LESO-based vibration controllers in almost every frequency range, because the nonlinear ESO has the advantages of peaking values and noise tolerance for systems nonlinearity. From the experimental results shown in Fig. 9, it is also illustrated that the whole performance of vibration suppression by the enhanced TDCNESO-based vibration controller is the best, because the proposed enhanced time delay compensator can also improve the performance of the NESO with a lower driven voltage. It follows from Fig. 10, especially Fig. 10(b) that the driven voltages of the piezoelectric bimorph under the NESO-based vibration controller are much lower than LESO-based controllers.

Following the driven voltages of Fig. 10 and experimental results in Fig. 10(b), it can be seen that the amplitude values of first mode of the piezoelectric plate under the proposed enhanced TDCNESO-based vibration controller is reduced by 15.87dB, which is better than that under NESO-based vibration controller (15.86dB), enhanced TDCLESO-based vibration controller (15.47dB), and LESO-based vibration controller (14.33dB). At the same time, the amplitudes from two to six times of the first natural modal frequency under the enhanced TDCNESO-based vibration controller are reduced by 26.25dB (at 113.6Hz), 19.71dB (at 169.7Hz), 9.29dB (at 225.9Hz), 17.78dB (at 282.1Hz), 24.17dB (at 339.5Hz), 15.7dB (at 395.6Hz), which are also better than the NESO-based controller (23.18dB, 20.02dB, 2.13dB, 15.11dB, 12.06dB, 13dB, respectively) measured by the accelerometer in Figs. 10(b) to (f). It, therefore, can be seen from the experimental results that the vibration suppression performances under NESO-based controllers are superior than the LESO-based controllers in almost entire frequency domain in this paper, because the whole vibration control system is affected by high harmonic frequency caused by the nonlinear vibration of the all-clamped piezoelectric thin plate structural vibration system.

Table 3 Comparisons of vibration suppression performances

Frequency (Hz)	Without control (dB)	LESO-based controller (dB)	NESO-based controller (dB)	Enhanced TDCLESO-based controller (dB)	Enhanced TDCNESO-based controller (dB)
56.17	0.51	-13.82	-15.35	-14.96	-15.36
113.6	-30.09	-44.21	-53.27	-43.52	-56.34
169.7	-16.99	-27.93	-37.01	-27.9	-36.7
225.9	-55.66	-38.28	-57.79	-37.25	-64.95
282.1	-49.09	-48.31	-64.2	-46.45	-66.87
339.5	-52.24	-57.33	-65.1	-53.24	-76.41
395.6	-54.82	-61.95	-67.82	-63.2	-70.52

The vibration suppression performance of the four different ESO-based controllers are summarized in **Table 3**. From the experimental results and **Table 3**, it is easily obtained that the enhanced time delay compensator can improve the vibration suppression performances of the LESO-based and NESO-based controllers, because the time delay is considered in the control design. Although a contradictory experimental result is indicated that the vibration suppression performance under the LESO-based controller is a little better than that under the enhanced TDCLESO-based controller from Figs. 9 (d) to (f), further analysis of Fig.

10(b) shows that the driven voltage value under the enhanced TDCLESO-based controller is lower than that under the LESO-based controller. In addition, the experimental results of NESO-based controllers are better than the enhanced TDCLESO-based controller in a wide frequency range. It also shows that LESO-based controllers have certain ability in dealing with the problems of nonlinearity and high frequency harmonics in structural vibration suppression. However, it is noted that the NESO-based controllers possess more advantages in dealing with these problems. That is to say the LESO-based controller has a certain time delay margin and high harmonics tolerance with the well-tuned parameters, but the vibration suppression performance under the two LESO-based controllers are relatively limited in this paper. So, the nonlinear approaches are required to improve the control performance with the proposed enhanced time delay compensator. Moreover, from the proposed enhanced TDCNESO-based controller with the novel differentiator, excellent vibration suppression performance for the all-clamped piezoelectric thin plate is achieved because of its strong disturbance rejection abilities. Thus, for structural vibration problems with a variety of internal and external disturbances, time delay and complex boundary conditions, etc, the NESO-based controllers, especially the proposed enhanced TDCNESO-based controller with the novel differentiator method, have higher efficiency and perfect vibration suppression performance.

Finally, the proposed enhanced TDCNESO-based controller is compared with two classical active vibration control methods, i.e., velocity feedback and PID controller. The three controllers are applied to the same all-clamped piezoelectric plate structure excited by a force vibrator for a fair comparison. The control gain of velocity feedback is 3, and the controller parameters of PID are proportional gain, integral gain, and derivative gain of 0.75, 0.0175, and 0.043 respectively. The time and frequency domain responses of the uncontrolled and three vibration controllers for the all-clamped piezoelectric plate structure are shown in Figs. 11 and 12, respectively. The driven voltages of the piezoelectric bimorph actuator under the three vibration controllers are shown in Fig. 13. The experimental results in Figs. 11 and 12 (a)-(b) indicate that although the three controllers have the effect of vibration isolation, the proposed method has a lower amplitude driven voltage while having a better vibration suppression performance. Therefore, it can be concluded that the enhanced TDCNESO-based vibration control scheme is an effective method to suppress structure vibrations.

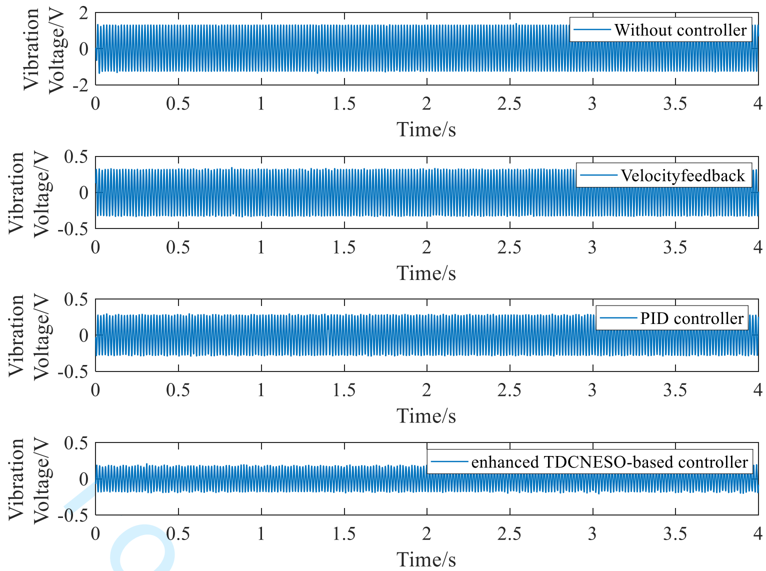

Fig. 11 Vibration suppression performance comparisons in time domain under velocity feedback, PID controller and the proposed enhanced TDCNESO-based controller.

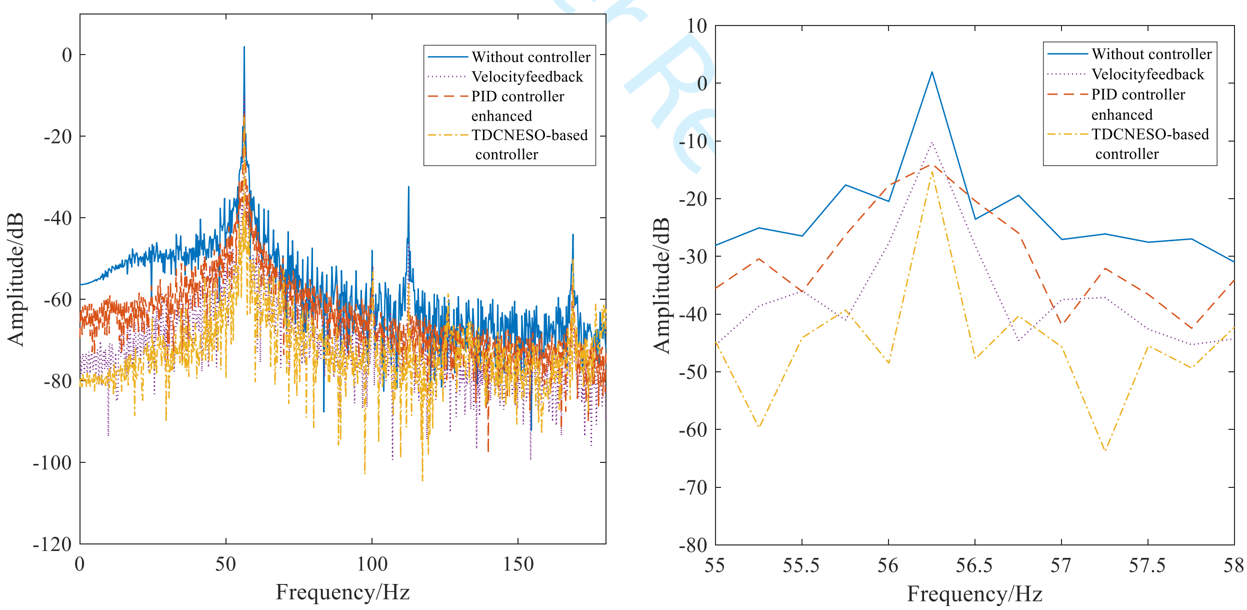

(a) Global response curves (b) Local curves close to frequency 56.2Hz

Fig. 12 Vibration suppression performance comparisons in frequency domain under velocity feedback, PID controller and the proposed enhanced TDCNESO-based controller.

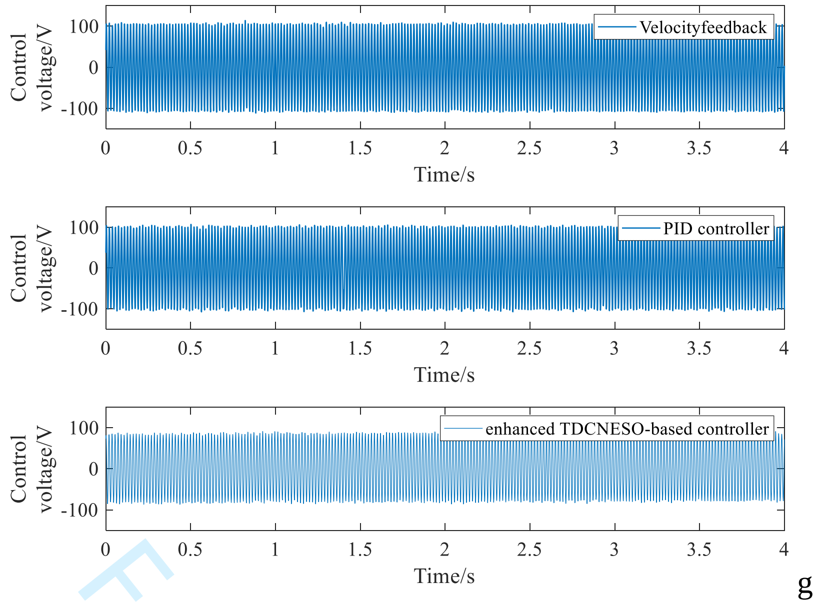

Fig. 13 Piezoelectric bimorph driven voltages under velocity feedback, PID controller and the proposed enhanced TDCNESO-based controller.

V. CONCLUSION

This work considers the vibration suppression problem for an all-clamped piezoelectric plate in the presence of various disturbances and time delay. Although LESO-based controllers have the tolerance of the time delay margin and excellent anti-disturbance ability for structural vibration control system with complex boundary conditions, the vibration suppression performance may be degraded when the practical piezoelectric thin plate structure is subjected to disturbances, time delay, and high harmonics, simultaneously. To achieve improved performance, an enhanced time delay compensator with a novel differentiator is developed to improve the ESO-based controllers. An interesting phenomenon is shown in the experiment that several times of the first mode natural frequency are excited by the first mode natural frequency signal in this paper. Considering the nonlinearity caused by the two to six times of 1st natural frequency of the all-clamped thin plate structure, the nonlinear ESO-based controller is more suitable for addressing the problem, since the peaking values and noise tolerance of NESO-based controller are better than LESO-based controller with the similar bandwidth tuning parameters. The proposed enhanced TDCNESO-based controller is compared against three existing ESO-based controllers, velocity feedback controller and the traditional PID method by using real-life experiments on the all-clamped piezoelectric plate. The comparative experimental results validate the effectiveness and superiority of the proposed methods. First the two NESO-based controllers with lower driven voltages have better vibration suppression performances than the two LESO-based controllers. The experimental results also show that the vibration suppression performance of the proposed enhanced TDCNESO-based controller is better than the NESO-based controller, so it is proved that the proposed enhanced time delay compensator can significantly improve the vibration suppression performance of the NESO-based controller in the present of time delay and total disturbances, simultaneously. Therefore, in order to improve the control performance of time delay systems, in practical vibration suppression systems, the NESO-based controller should be embedded the structure and parameters of the time delay compensation method selected reasonably.

Although comparative experiments improve the effectiveness and superiority of the developed enhanced TDCNESO-based controller, there is still room for further development. First, considering the recent research results in structural vibration control system, the main source of time delay is the arrangement of actuators and sensors, so how to arrange the pairs of actuators and sensors to reduce the system delay is a very important research direction. Second, this work provides practitioners with vital guidance in designing active vibration control system in the presence of disturbances and time delay, mainly from the experimental point of view, while it is also very important to explain the advantages of the enhanced TDCNESO-based controller from the perspective of control theory. Third, we will also consider actuator and sensor faults, input saturation and input delay simultaneously in the future.

Acknowledgements

This work was supported in part by the National Natural Science Foundation of China (Grant nos. 61903322, 61773335), State Key Laboratory of Mechanics and Control of Mechanical Structures (Grant No. MCMS-E-0520G01), Six Talent Peaks Foundation of Jiangsu Provincial (Grant no. KTHY2018038).

Declaration of conflicting interests

The author(s) declared no potential conflicts of interest with respect to the research, authorship, and/or publication of this article.

Appendix

Coefficients in L(s)

$$L_{n0} = 127.24\beta_{03} \quad L_{n1} = 127.24\beta_{03}k_d \quad L_{n2} = 127.24\beta_{03}k_p$$

$$L_{d0} = \hat{c}_0 \; L_{d1} = \hat{c}_0(2.957 + k_d + \beta_{01}) \; L_{d2} = \hat{c}_0(153500 + \beta_{01}k_d + k_p + \beta_{02} + 2.957\beta_{01} + 2.957k_d)$$

$$L_{d3} = \hat{c}_0(153500\beta_{01} + 153500k_d + 2.957\beta_{01}k_d + 2.957k_p + 2.957\beta_{02}) + 127.24\beta_{01}k_p + 127.24\beta_{02}k_d$$

$$L_{d4} = 153500\hat{c}_0(\beta_{01}k_d + k_p + \beta_{02}) + 127.24\beta_{02}k_p$$

References

Anik P, Philippe M and Alain B. (2018) Harmonic active vibration control using piezoelectric self-sensing actuation with complete digital compensation. *Journal of intelligent material systems and structures*, 29(7):1510-1519.

Caruso G. (2001) A critical analysis of electric shunt circuits employed in piezoelectric passive vibration damping. *Smart materials and structures*, 10: 1059-1068.

Castaneda LA, Luviano-Juarez A, Ochoa-Ortega G, et al. (2018) Tracking control of uncertain time delay systems: An ADRC approach. *Control Engineering Practice*, 78: 97-104.

Chen S, Xue WC and Huang Y (2019) Analytical design of active disturbance rejection control for nonlinear uncertain system with delay. *Control Engineering Practice*, 84: 323-336.

Chen S, Xue WC, Zhong S, et al. (2018) On comparison of modified ADRCs for nonlinear uncertain systems with time delay. *Science China-Information Sciences*, 61(7), DOI: 10.1007/s11432-017-9403-x.

Geng XP, Liu T, Hao SL, et al. (2019). Anti-windup design of active disturbance rejection control for sampled systems with input delay. *International Journal of Robust and Nonlinear Control*, 30(3): 1311-1327.

Gozum MM, Aghakhani A and Serhat G. (2018) Electroelastic modeling of thin-laminated composite plates with surface-bonded piezo-patches using Rayleigh-Ritz method. *Journal of intelligent material systems and structures*, 29(10):2192-2205.

Guzman DG, Silva ECN and Rubio WM (2020) Topology optimization of piezoelectric sensor and actuator for active vibration control. *Smart Materials and Structures*, 29(8): 085009.

Han JQ (2009) From PID to active disturbance rejection control. *IEEE Transactions on Industrial Electronic*s, 56(3): 900-906.

He Y, Chen XA, Liu Z, et al. (2019) Active vibration control of motorized spindle based on mixed H infinity/Kalman filter robust state feedback control. *Journal of Vibration and Control*, 25(6): 1279-1293.

Hu KM and Li H (2018) Multi-parameter optimization of piezoelectric actuators for multi-mode active vibration control of cylindrical shells. *Journal of Sound and Vibration*, 426: 166-185.

Kant M and Parameswaran AP (2018) Modeling of low frequency dynamics of a smart system and its state feedback based active control. *Mechanical Systems and Signal Processing*, 99: 774-789.

Kim B, Washington GN and Yoon HS (2013) Active vibration suppression of a 1D piezoelectric bimorph structure using model predictive sliding mode control. *Smart Structures and Systems*, 11(6): 623-635.

Language JY, Liang WY and Tan KK (2020) Motion control or piezoelectric-actuator-based surgical device using neural network and extended state observer. *IEEE Transactions on Industrial Electronics*, 67(1): 402-412.

Li SQ, Li J and Mo YP (2014a) Piezoelectric multimode vibration control for stiffened plate using ADRC-based acceleration. *IEEE Transactions on Industrial Electronics*, 61(12): 6892-6902.

Li SQ, Li J, Mo YP, et al. (2014b) Composite multi-modal vibration control for a stiffened plate using non-collocated acceleration sensor and piezoelectric actuator. *Smart Materials and Structures*, 23(1), DOI: 10.1088/0964-1726/23/1/015006.

Li J, Qi XH, Xia YQ, et al. (2015) Frequency domain stability analysis of nonlinear active disturbance rejection control system[J]. *ISA Transactions*. DOI: 10.1016/j.isatra.2014.11.009.

Li S, Qiu J, Li J, et al. (2012) Multi-modal vibration control using amended disturbance observer compensation. *IET Control Theory and Applications*, 6(1): 72-83.

Li SQ, Zhu CW, Mao QB, et al. (2021) Active disturbance rejection vibration control for an all-clamped piezoelectric plate with delay. *Control Engineering Practice*, 108, DOI: 10.1016/j.conengprac. 2020.104719.

Ling J, Feng Z, Kang X, et al. (2020) Bandwidth enhancement in damping control for piezoelectric nanopositioning stages with load uncertainty: design and implementation. *Journal of Vibration and Control*, DOI:10.1177/1077546320941705.

Liu JJ, Sun MW, Chen ZQ, et al. (2020) Super-twisting sliding mode control for aircraft at high angle of attack based on finite-time extended state observer. *Nonlinear Dynamics*, 99 (4): 2785-2799.

Liu T, Hao SL, Li DW, et al. (2019) Predictor-based disturbance rejection control for sampled systems with input delay. *IEEE Transactions on Control Systems Technology*, 27(2): 772-780.

Luo YJ, Zhang X, Zhang YH, et al. (2018) Active vibration control of a hoop truss structure with piezoelectric bending actuators based on a fuzzy logic algorithm. *Smart Materials and Structures*, 27(8): 085030.

Muc A, Flis J and Augustyn M (2019) Optimal design of plated/shell structures under flutter constraints- A literature review. *Materials*, 12(24): 4215.

Oveisi A, Hosseini-Pishrobat M, Nestorovic T, et al. (2018) Observer-based repetitive model predictive control in active vibration suppression. *Structural Control & Health Monitoring*, 25(5), DOI: 10.1002/stc.2149.

Overschee PV and Moor BD (1996) Subspace identification for linear systems: Theory implementation applications. Kluwer Academic Publishers, Dordrecht.

Pawar SN, Chile RH and Patre BM (2017) Modified reduced order observer based linear active disturbance rejection control for TITO systems. *ISA Transactions*, 71: 480-494.

Pu YX, Zhou HL and Meng Z (2019) Multi-channel adaptive active vibration control of piezoelectric smart plate with nonlinear secondary patch modelling using PZT patches. *Mechanical Systems and Signal*

Processing, 120: 167-179.

Qiu ZC, Han JD, Zhang XM, et al. (2009) Active vibration control of a flexible beam using a non-collocated acceleration sensor and piezoelectric patch actuator. *Journal of Sound and Vibration*, 326(3-5): 438-455.

Qiu ZC, Wang TX and Zhang XM. (2021) Sliding mode predictive vibration control of a piezoelectric flexible plate. *Journal of intelligent material systems and structures.* 32(1): 65-81.

Ran MP, Wang Q, Dong CY, et al. (2020) Active disturbance rejection control for uncertain time-delay nonlinear systems. *Automatica*, 112, DOI: 10.1016/j.automatica.2019.108692.

Rezaee M, Jahangiri R and Shabani R (2019) Robust adaptive fuzzy sliding mode control of nonlinear uncertain MIMO fluttering FGP plate based on feedback linearization. *Aerospace Science and Technology*, 91: 391-409.

Sun N, Wu YM, Fang YC, et al. (2018) Nonlinear antiswing control for crane systems with double-pendulum swing effects and uncertain parameters: design and experiments. *IEEE Transactions on Automation Science and Engineering*, 15(3): 1413-1422.

Tomas RC, Carla MR and Pedro R. (2018) Active vibration control of piezoelectric smart beams with radial basis function generated finite difference collocation method. *Journal of Intelligent Material Systems and Structures*, 29(13):2728-2743.

Wang S, Chen ZB, Liu XX, et al. (2018) Feedforward Feedback linearization linear quadratic Gaussian with loop transfer recovery control of piezoelectric actuator in active vibration isolation system. *Journal of Vibration and Acoustics-Transactions of The ASME*, 140(4): 041009.

Wu D and Chen K. (2013) Frequency-Domain Analysis of Nonlinear Active Disturbance Rejection Control via the Describing Function Method. *IEEE Transactions on Industrial Electronics*, 60(9):3906-3914.

Wu D and Chen K. (2014) Limit cycle analysis of active disturbance rejection control system with two nonlinearities[J]. *ISA Transactions*, 53(4):947-954.

Xu QS and Li YM (2012) Model predictive discrete-time sliding mode control of a nanopositioning piezostage without modeling hysteresis. *IEEE Transactions on Control Systems Technology*, 20(4):

983-994.

Yousefpour A, Hosseinloo AH, Yazdi M, et al. (2020) Disturbance observer–based terminal sliding mode control for effective performance of a nonlinear vibration energy harvester. *Journal of Intelligent Material Systems and Structures*, 31(12):1495-1510.

Zhang C, Ma GF, Sun YC, et al. (2019) Prescribed performance adaptive attitude tracking control for flexible spacecraft with active vibration suppression. *Nonlinear Dynamics*, 96(3): 1909-1926, 2019.

Zhang M and Jing X (2020) A bioinspired dynamics-based adaptive fuzzy SMC method for half-car active suspension system with input dead zones and saturations. *IEEE Transactions on Cybernetics*, DOI: 10.1109/TCYB.2020.2972322.

Zhang SQ, Li HN, Schmidt R, et al. (2014) Disturbance rejection control for vibration suppression of piezoelectric laminated thin-walled structures. *Journal of Sound and Vibration*, 333(5): 1209-1223.

Zhang SQ, Zhao GZ, Rao MN, et al. (2019) A review on modeling techniques of piezoelectric integrated plates and shells. *Journal of Intelligent Material and Structures*, 30(8): 1133-1147.

Zhao ZL and Guo BZ (2017) A nonlinear extended state observer based on fractional power functions. *Automatica*, 81:286-296.

Zhao ZL and Guo BZ (2018) A novel extended state observer for output tracking of MIMO systems with mismatched uncertainty. *IEEE Transactions on Automatic Control*, 63(1): 211-218.

Zheng QL, Richter H and Gao ZQ (2014) Active disturbance rejection control for piezoelectric beam. *Asian Journal of Control*, 16(6): 1612-1622